Discretizing low-intensity whole-body vibration into bouts with short rest intervals promotes bone defect repair in osteoporotic mice

Takeshi Matsumoto, Keishi Hashimoto, Hyuga Okada

Graduate School of Technology, Industrial and Social Sciences, Tokushima University

Corresponding author: Takeshi Matsumoto

Graduate School of Technology, Industrial and Social Sciences, Tokushima University

2-1 Minamijyousanjima-cho, Tokushima 770-8506, Japan

Tel./fax: +81 886567374; E-mail: t.matsumoto@tokushima-u.ac.jp

Running title: Vibration bouts with short rests

Author Contributions Statement

Takeshi Matsumoto: study design, funding acquisition, supervision, data collection, data analysis, drafting of the manuscript, review of the manuscript. Keishi Hashimoto: data collection, data analysis, drafting of the manuscript, review of the manuscript. Hyuga Okada: data collection, data analysis, review of the manuscript. All authors approved the final submitted manuscript.

Abstract

Continuous administration of low-intensity whole-body vibration (WBV) gradually diminishes bone mechanosensitivity over time, leading to a weakening of its osteogenic effect. We investigated whether discretizing WBV into bouts with short rest intervals was effective in enhancing osteoporotic bone repair. Ten-week-old female mice were ovariectomized and underwent drill-hole defect surgery (day 0) on the right tibial diaphysis at 11 weeks of age. The mice underwent one of three regimens starting from day 1 for 5 days/week: continuous WBV at 45 Hz and 0.3 g for 7.5 minutes/day (cWBV); 3-second bouts of WBV at 45 Hz, 0.3 g followed by 9-second rest intervals, repeated for 30 minutes/day (rWBV); or a sham treatment. Both the cWBV and rWBV groups received a total of 20,250 vibration cycles per day. On either day 7 or 14 post-euthanasia (n = 6/group/timepoint), the bone and angiogenic vasculature in the defect were CT imaged using synchrotron lights. By day 14, the bone repair was most advanced in the rWBV group, showing a higher bone volume fraction and a more uniform mineral distribution compared with the sham group. The cWBV group exhibited an intermediate level of bone repair between the sham and rWBV groups. The rWBV group had a decrease in large-sized angiogenic vessels, while the cWBV group showed an increase in such vessels. In conclusion, osteoporotic bone repair was enhanced by WBV bouts with short rest intervals, which may potentially be attributed to the improved mechanosensitivity of osteogenic cells and alterations in angiogenic vasculature.

Keywords: osteoporosis, bone repair, mechanosensitivity, angiogenic vasculature

1. INTRODUCTION

As a corollary of the aging global population, osteoporosis has become an important healthcare issue for millions of older adults, predominantly postmenopausal women. The risk of future immobilization in postmenopausal Japanese women is reported to increase by 1.83-fold with osteoporosis.[1] The most prevalent complication of osteoporosis is fracture, which affects one in three women and one in five men aged 50 years and over worldwide.[2] It is well documented that the fracture healing process is impaired in rodent models of osteoporosis by ovariectomy (OVX).[3–5] Impaired bone healing may prolong bed rest or physical immobility, induce deconditioning and motor deterioration, and result in severe secondary complications that require long-term nursing care, or even lead to in-hospital death.[6,7] It is vital to enhance osteoporotic fracture healing, thereby achieving early remobilization, to avoid osteoporotic patients being bedridden or in need of nursing care.

Bone regenerative capacity is mechanically stimulus-dependent, and moderate loading accelerates the healing of fractures.[8,9] Therefore, the application of mechanical stimuli soon after fracture treatment may accelerate the healing of osteoporotic fractures toward the early achievement of structural resistance needed to undergo rehabilitation.[10] One mechanical modality available during the early stage of fracture healing is low-intensity whole-body vibration (WBV), with its frequency and magnitude generally ranging from 20–100 Hz and < $1 \times g$ (= 9.81 m/s^2), respectively. Mechanical stimuli of WBV safely propagate to bone tissue wherein low strains (< 10 με) and high-frequency accelerations arise, increasing the osteogenic capacity of osteoblasts and bone marrow mesenchymal stem cells (MSCs).[11,12] Bone strain dynamics induced by WBV are comparable with those attributed to postural muscle activity,[13,14] thereby enabling WBV to serve as a safe passive exercise suitable for osteoporotic patients. Numerous animal studies have demonstrated the efficacy of WBV for healing osteoporotic fractures,[15] which relies on estrogen receptor α-signaling under estrogen deficiency.[16] Furthermore, WBV improves angiogenic vascularization in osteoporotic fractures.[17,18] Angiogenesis within bone injury is essential in early stage healing to provide a supply route of oxygen and nutrients necessary for high metabolic activity in osteoblasts, as well as a migration route for MSCs and a source of bone growth factors that mediate osteoblastic differentiation.[19–21]

Bone sensitivity to WBV decreases with long-term exposure, as implied by the absence of bone gains in the spine or hip of postmenopausal women with increased exposure duration to WBV.[22] Such desensitization to mechanical stimuli has been observed in a load-induced osteogenic response, which is sharply blunted after the first few load cycles.[23]

However, it has been reported that intervals inserted between each period of mechanical stimuli, even short intervals, are effective in maintaining bone mechanosensitivity. A 10-second interval following each single bending load cycle (0.25 N peak) enhances osteogenesis to a similar degree as continuous loading under magnitudes 10 times greater in turkey ulnae.[24] Additionally, rat tibiae subjected to single-loading in bending (54 N peak) at 14-second intervals show elevated bone formation rates relative to those subjected to the same number of loading cycles without intervals, while those single-loaded at intervals of ≤ 7 seconds do not.[25] Rest insertion is also favorable for osteogenesis in high-frequency loading regimes; 1-second bouts of 30-Hz loading applied at 10-second intervals in bending at peak of 800 microstrains exerts a greater bone-anabolic effect on mouse tibiae than continuous 30-Hz loading, despite a 10-fold reduction in the total number of loading cycles.[26] Thus, although bone deformation induced by these rest-inserted mechanical stimuli is not at the microstrain level observed in bone exposed to WBV,[27,28] it is anticipated that bouts of WBV with short rest intervals might be more bone-anabolic than continuous WBV and may be effective for the treatment of osteoporotic fractures.

It is of value to confirm whether WBV bouts with short rest intervals effectively enhance osteoporotic fracture healing. However, to our knowledge, no data have been presented on the benefits of incorporating short rest periods in the WBV treatment of osteoporotic fracture. Therefore, this study was performed to test the hypothesis that WBV in bouts with short rest intervals augments its effectiveness for bone defect repair in OVX mice. In addition, we investigated the effect of short rest insertion within WBV on vascular ingrowth, which is essential for bone healing.

2. MATERIALS AND METHODS

The protocol for the animal treatment was in accordance with the guiding principles of the Care and Use of Laboratory Animals of Tokushima University and was approved by the Ethics Committee on Animal Experiments of Tokushima University (permit no. T2020-126).

2.1 Animal model and experimental design

Thirty-six female C57BL/6JJcl mice (CLEA Japan, Tokyo, Japan), which is an inbred strain exhibiting highly mechanosensitive bones,[29] were bilaterally ovariectomized under anesthesia induced by an intraperitoneal injection of ketamine (100 mg/kg) and xylazine (10 mg/kg) at the age of 10 weeks. One week later, the mice were anesthetized with isoflurane, and the skin over the medial aspect of the right lower leg was shaved, swabbed with povidone-iodine, and incised. A full-thickness unicortical hole was created approximately 2 mm proximal to the tibia-fibula junction using a 0.5-mm diameter drill rotating at 11,000 rpm (Muromachi Kikai, Kyoto, Japan). Drill margins were frequently irrigated with saline to avoid thermal necrosis and remove bone fragments.

The day after drill-hole surgery (day 0), the mice were randomly divided into three groups (n = 12 per group) and treated for 5 days/week as follows. The continuous WBV group (cWBV) were subjected to WBV at 45 Hz, 0.3 g (0-to-peak) continuously for 7.5 minutes/day; the rest-inserted WBV group (rWBV) were subjected to 3-second bouts of WBV at 45 Hz, 0.3 g followed by 9-second rest intervals, repeated for 30 minutes/day; and the sham-treated group (sham) were treated similarly for 7.5 minutes but without vibration exposure. Both the cWBV and rWBV groups received 20,250 total vibration cycles per day.

Four mice at a time were placed in a compartmentalized cage that was firmly fixed by screws to a rigid vibration platform.[30] The platform was driven by an electromagnetic actuator connected to a power supply/amplifier/controller (Big-Wave; Asahi Seisakujo, Tokyo, Japan). Using data received from an accelerometer attached to the platform, the vibration controller produced the required sine-wave vibration. All mice were routinely treated between 10:00 and 11:00.

During the experimental period, the mice were single-housed in plastic cages under controlled conditions (12-hour light/dark cycle, 25°C, 60% humidity) and allowed free access to a standard diet (CE-2; CLEA Japan) and tap water.

2.2 Sample preparation

On post-surgery days 7 and 14, six mice per group on each day of observation underwent vascular casting as described elsewhere.[31] Briefly, under isoflurane anesthesia, mice were thoracotomized and a polyethylene catheter was inserted into the left ventricle. Following isoflurane overdose for euthanasia, the right atrium was cut open and the vascular bed was flushed with heparinized saline and then with phosphate buffer solution into the left ventricle. The vascular bed was then thoroughly perfused with an agarose suspension of zirconium dioxide submicron particles (ZrCA) at 120 mmHg. The mice were laparotomized for clamping of the abdominal artery and vein and immersed in an ice-cold water bath for 1 hour. The right tibia with the drilled defect was harvested and fixed in 4% paraformaldehyde until CT scanning.

2.3 Synchrotron radiation-based subtraction computed tomography

Each specimen, while immersed in 4% paraformaldehyde, was scanned at beamline 20B2 of SPring-8 (Harima, Japan) using monochromatic synchrotron lights just above (18.05 keV) and below (17.95 keV) the K edge of ZrCA. A scientific CMOS camera (C11440-22C; Hamamatsu Photonics, Hamamatsu, Japan) combined with a beam monitor (BM2; Hamamatsu Photonics) with a 10-µm-thick phosphor screen ($Gd_2O_2S:Tb+$) was used to detect transmitted X-rays. Scanning was performed over an angular range of 0–180° at 0.1° with a

0.2-second exposure per frame. After corrections for X-ray source instability and detector background, each scan dataset was reconstructed with a two-dimensional filtered backward projection algorithm provided by SPring-8, yielding a two-dimensional image stack composed of 2.75-μm cubic voxels in 8-bit grayscale.

The 17.95- and 18.05-keV images were calibrated to enhance the vascular contrast in 18.05-keV images through the ZrCA K-edge effect and to reduce the bone contrast in both images to the same gray levels by matching the range of the linear absorption coefficient (μ, /cm) of 0 to 40/cm with the full grayscale range of 0 [black] to 255 [white]. Thereby, selective visualization of vascular structure was possible by subtraction between a pair of 17.95- and 18.05-keV images.[31] The vascular image yielded by image subtraction was filtered by 3 × 3 × 3 voxels averaging and binarized using Otsu's thresholding method.

Bone was segmented from the 17.95-keV image after calibrating to match the μ range of 0 to 14/cm with the full grayscale and subtracting the binarized vascular image obtained in advance. The use of monochromatic synchrotron light made it possible to translate the reconstructed image into the distribution of bone mineral density (ρ, g/cm^3) based on the equation: $\mu = 7.58 \times \rho + 1.03$ ($r^2 > 0.999$), which was obtained from the 17.95-keV scan dataset of K_2HPO_4 phantom solutions (0–1 g/mL). All voxels of $\mu > 4.82$/cm, equivalent to $\rho > 0.5$ g/cm^3, were classified as bone. A custom C program and ImageJ 1.54b software were used for this series of image processing.

2.4 Quantitative parameters for bone and vascular structures

A cylindrical region of interest (diameter, 495 µm; height, 110 µm) was chosen in the cortical defect. The thickness was less than but close to the thickness of a nearby intact cortical bone. The bone volume fraction (B.Vf, %), bone thickness (B.Th, µm), bone spacing or thickness of the background (B.Sep, µm), vascular volume fraction (V.Vf, %), vessel thickness (V.Th, µm), and number density of node-to-node or node-to-free-end vessel segments (V.N, /mm^3) were calculated. The BoneJ plugin 1.3.5 for ImageJ[32] was used to determine all indices, except for V.Th. For calculating V.Th, the local thickness was first calculated as the diameter of the largest sphere falling inside the vascular space with its center on a vascular skeleton line provided by a thinning algorithm. Then, V.Th was determined as an average of these thicknesses on overall skeleton lines. The thickness of each vessel segment also was determined as an average of local vessel thicknesses over its skeleton line, and size-specific V.N was calculated. Using the linear µ-ρ relation, local ρ values were determined for newly formed bone.

2.5 Statistical analysis

The data are expressed as means ± SD except for ρ frequency distribution, in which means ± SE are shown for clarity. Non-parametric statistical analysis was performed because the Kolmogorov–Smirnov test determined that the data of some experimental groups were not normally distributed. The Kruskal-Wallis test followed by the two-tailed Dunn's post hoc test were used to identify statistically significant differences between the sham, cWBV, and rWBV groups. Intragroup differences were assessed using the two-tailed Mann–Whitney U test and the two-tailed Wilcoxon signed-rank test for independent and paired data, respectively. All data were analyzed by Prism 8 (GraphPad Software; San Diego, CA). $P < 0.05$ was considered statistically significant.

3. RESULTS

The mean body weights in the sham, cWBV, and rWBV groups, respectively, were 20.8 ± 0.8, 20.7 ± 1.0, and 20.5 ± 1.0 g on day 0, 21.8 ± 0.8, 21.0 ± 1.1, and 21.2 ± 0.8 g on day 7, and 20.8 ± 0.8, 21.0 ± 0.6, and 20.7 ± 0.8 g on day 14. Body weight did not change over time or differ between the groups. All animals were included in each analysis.

Three-dimensional reconstruction of microstructure in the bone defect is exemplified for each group on each observation day in Figure 1. The structural bone and vasculature parameters are shown in Tables 1 and 2. On day 7, newly formed bone appeared with vascular ingrowth in each group, filling the defect with a higher proportion of woven-like bone than with blood vessels (B.Vf > V.Vf). At this stage, there were no differences between the three groups in any of the bone and vascular structure parameters. From days 7 to 14, B.Vf and B.Th increased in every group, while B.Sep increased in the sham and cWBV groups but not in the rWBV group. Vascular ingrowth progressed to regression. V.Th decreased in the sham and rWBV groups, while V.N decreased in the cWBV and rWBV groups. On day 14, as a result of advanced bone repair, the rWBV group had a higher B.Vf and lower B.Sep than the sham group. The rWBV group had a smaller V.Th than the cWBV group.

The percent frequencies of bone mineral density within the defects on days 7 and 14 are shown in Figure 2. On day 7, there was no difference in distribution between the three groups. The mean and median values, respectively, were 0.685 ± 0.024 and 0.670 ± 0.028 g/cm^3 in the sham group, 0.673 ± 0.032 and 0.647 ± 0.022 g/cm^3 in the cWBV group, and 0.693 ± 0.033 and 0.652 ± 0.019 g/cm^3 in the rWBV group. From days 7 to 14, the distribution changed from monotonically decreasing to unimodal. The mean and median values, respectively, on day 14 were 0.935 ± 0.047 and 0.970 ± 0.053 g/cm^3 in the sham group, 0.932 ± 0.028 and 0.979 ± 0.031 g/cm^3 in the cWBV group, and 0.953 ± 0.039 and 0.994 ± 0.037 g/cm^3 in the rWBV group. Each distribution peaked at a similar value, but the negative skewness tended to be larger in the rWBV group than in the sham group (-0.590 ± 0.238 vs. -0.863 ± 0.169, $P = 0.080$). Furthermore, the coefficient of variations was significantly smaller in the rWBV group than in the sham group (0.174 ± 0.008 vs. 0.190 ± 0.009, $P < 0.05$). The kurtosis did not differ between the three groups.

Figure 3 shows V.N for the thicknesses of < 11.0 and > 11.0 μm on days 7 and 14. On day 7, V.N was higher for the > 11.0 μm thickness than the < 11.0 μm thickness in the cWBV group, and V.N for the > 11.0 μm thickness tended to be higher in the sham group ($P = 0.0625$) and the rWBV group ($P = 0.0938$). No intergroup difference in V.N was observed for either of the two thickness ranges. From day 7 to 14, V.N for the < 11.0 μm thickness tended to decrease in the rWBV group (P = 0.0931), while V.N for the > 11.0 µm thickness decreased in the rWBV group and tended to decrease in the cWBV group (P = 0.0649). On day 14, V.N was higher for the > 11.0 µm thickness than the < 11.0 µm thickness in the sham and cWBV groups but was similar between the two thickness ranges in the rWBV group. Although V.N for the < 11.0 µm thickness was similar between the groups, V.N for the > 11.0 µm thickness was smaller in the rWBV group than in the cWBV group.

Figure 4 shows the percentage of vessel number density (%V.N) for seven (day 7) or eight (day 14) thickness ranges. On day 7, all groups showed a similar %V.N distribution with a peak in the thickness range of 11.0–16.5 µm, and there were no differences between the three groups in any size-specific %V.N. On day 14, the rWBV group had a higher %V.N and a trend toward a higher %V.N for the < 11.0 µm thickness than the cWBV group and the sham group (P = 0.080), respectively. In contrast, the cWBV group had a higher %V.N than the sham group in the thickness ranges of 33.0–44.0 and 38.5–44.0 µm and had a higher %V.N than the rWBV group in the thickness range of 38.5–44.0 µm. These differences in size-specific %V.N indicate that the size of angiogenic vessels was more uniform around the microvessels (< 11.0 µm) in the rWBV group than in the other groups.

4. DISCUSSION

The present study tested the hypothesis that discretizing WBV into short bouts by inserting short rest intervals is beneficial in promoting osteoporotic bone repair. Using synchrotron radiation CT combined with vascular casting, we demonstrated the efficacy of WBV bouts with short rest intervals for healing tibial drill-hole injuries in OVX mice. This effect was accompanied by modifications to the angiogenic vasculature, characterized by the reduction in large-sized vessels. Even when performed with the same total number of vibratory cycles as WBV bouts with short rest intervals, continuous WBV exhibited only intermediate effects on bone repair. Furthermore, continuous WBV led to an increase in large-sized vessels and an elevation of heterogeneity in angiogenic vasculature.

Despite inducing only extremely low bone strain, WBV is effective in enhancing osteoblastogenesis via canonical Wnt signaling.[11] Therefore, WBV is applicable for the treatment of osteoporotic fractures and has been shown to promote osteoporotic fracture healing in rodent models.[33,34] We found that the therapeutic effect of WBV was further enhanced by dividing it into short bouts administered intermittently with short intervals in between, similar to the increased osteogenesis obtained by inserting rest periods into the mechanical regime using larger stimuli.[24–26] In addition, although no effect was found on mean mineral density, WBV bouts with short rests resulted in greater negative skewness and a lower coefficient of variation of mineral distribution than continuous WBV, implying a faster progression of mineral maturation.

Low-intensity vibration directly stimulates bone marrow MSCs via downregulating adipogenic differentiation, and stimulates osteoblastic cells toward osteogenesis.[12,35–37] Despite receiving the same total vibratory stimuli, the promotion of bone repair was significant in the rWBV group but not in the cWBV group, implying the increased osteogenic activities of these cells owing to rest intervals. Although no studies have evaluated the efficacy of WBV discretization on osteogenic activity, one study investigated the significance of intermittent mechanical stimulation in fluid shear-induced calcium transients, an indicator of cell mechanosensitivity, in osteoblastic cells.[38] Osteoblastic cells exposed cumulatively for 3 minutes to 10-second durations of oscillatory flow (1 Hz at a peak shear stress of 1 or 2 Pa) with intervals of 10 or 15 seconds exhibit multiple calcium transients with increased magnitude and frequency and elevation of mRNA levels of osteopontin, compared with cells exposed to 3-minute continuous oscillatory flow.[38] Thus, the intermittent stimulation in the rWBV group may have improved the mechanosensitivity of osteogenic cells to WBV and led to the promotion of bone defect repair. Furthermore, it has been reported that even continuous oscillating flow (2 Hz at a peak shear stress of 2 Pa) may induce multiple calcium transients in osteoblastic cells after prolonged (15 minutes) exposure.[39] Indeed, bone repair in the drill-hole defect of mouse tibial bone is promoted by applying prolonged WBV (30 minutes/day, 30 Hz, 0.05 g).[28] However, the 7.5-minutes/day stimulation in the cWBV group may not be long enough to generate multiple calcium transients in osteoblastic cells, failing to improve the mechanosensitivity of osteogenic cells to WBV.

On days 7 and 14, the number density of angiogenic vessels with < 11 μm thickness did not differ between groups. In cranial bone defect repair, angiogenic vessels with < 10 μm thickness correlate with osteoblast volume better than those with > 10 μm thickness, and such close association of osteoblasts with capillary-sized vessels (angiogenesis-osteogenesis coupling) is suggested to be critical for bone repair.[40] Thus, we speculated that the angiogenesis-osteogenesis coupling was at a comparable level in all groups, at least concerning the number density of capillary-sized vessels. However, the number density of angiogenic vessels with > 11 μm thickness differed between the cWBV and rWBV groups on day 14. In the rWBV group, vessels with > 11 μm thickness decreased down to the number density of vessels with < 11 μm thickness from days 7 to 14, resulting in a reduced heterogeneity of vessel size distribution, with a predominance of vessels with < 11 μm thickness. The reduction in these large-sized vessels potentially suggests that vessels not contributing to perfusion throughout the defect were adaptively pruned.[41] In other words, WBV bouts with short rest intervals might facilitate the formation of more efficient and streamlined angiogenic vasculature. This modification to angiogenic vasculature besides the potential enhancement in mechanosensitivity of osteogenic cells may offer a rationale for the amelioration in osteogenic outcomes resulting from WBV bouts with short rest intervals. In contrast, in the cWBV group on day 14, many angiogenic vessels with > 11 μm thickness had not yet been pruned, and the proportion of large-sized vessels with a thickness of 33.0–44.0 μm was higher in the cWBV group than the other groups, indicating an increased heterogeneity of vessel size distribution. The large-sized vessels may act as shunts for blood flow, diminishing perfusion to small-sized vessels,[42] which could disturb the angiogenesis-osteogenesis coupling, consequently impeding the effects of WBV-induced mechanical stimulation on osteogenic cells. It was recently reported that VEGF-loaded fibrin gel added to a cortical defect promotes angiogenesis, especially in the formation of vessels with 5–30 μm thickness, and accelerates bone repair in a similar mouse model.[43] The enhancement of angiogenesis may potentially improve the outcomes of osteogenesis, depending on the distribution of vessel sizes.

The present findings contrast with those of a previous study that failed to show the benefits of WBV bouts with short rest intervals against decreasing the bone formation level in growing mice.[44] This discrepancy is affected by whether angiogenesis is essential to drive osteogenesis, as well as the difference in bone mechanosensitivity to WBV between OVX mice and growing male mice.[16,45] Furthermore, to maintain the same number of total vibratory stimuli in the previous study,[44] 1-second WBV bouts given at 10-second intervals needed 11 times longer experimental time than continuous WBV (165 vs. 15 minutes/day), whereas the rWBV group needed an experimental time that was four times longer than the cWBV group (30 vs. 7.5 minutes/day). Such prolonged animal restraint time accompanying the discretization of WBV as well as the different duration of each WBV bout (1 vs. 3 seconds) would affect the outcomes of WBV bouts with short rest intervals.

The present study has some limitations. The first limitation is the specificity of bone repair in the drill-hole defect model. Angiogenesis and osteogenesis are both influenced by WBV in a manner dependent on the degree of stability at injury sites, i.e., whether ossification is endochondral, intramembranous, or a combination of both. Thus, the actions of WBV on angiogenesis, osteogenesis, and their coupling likely differ between cortical drill-hole defect injury and clinically relevant orthopedic trauma. In the latter, enhanced angiogenesis accompanies the WBV-stimulated promotion of fracture repair.[17] Therefore, the bone repair is affected by the dynamics of mechanical properties at the fracture site, as well as the callus formation, and the presence of adjacent muscles. The second limitation is the lack of CT observation at varying stages of bone repair; in particular, we did not observe vascular invasion before or around the initiation of osteogenesis. In OVX mice, angiogenic vessels invade the cortical drill-hole defect 3 days after surgery,[46] and WBV may potentially influence the vasculature at this early stage, with consequences on osteogenesis thereafter. However, in the present study, no effect of WBV on angiogenesis or osteogenesis was observed on day 7. In an earlier study, dynamic tibial compression (2 Hz, 6 N, 120 cycles/day) applied from days 2 to 5 after tibial defect surgery had no effect on vessel population in the defect on day 10, although compression applied from days 5 to 8 led to an increase in vessels with approximately 10-μm thickness.[47] Thus, WBV applied in the phase dominated by angiogenesis may have less impact on the repair process. In this phase, the regenerated tissue in the defect is less solid due to the limited generation of extracellular matrix, which likely makes it less conducive to transmitting high-frequency vibrations. Finally, no mechanical property of regenerated bone was evaluated. Assessment of stiffness and toughness of regenerated bone is critical for enhancing the therapeutic value of WBV in fracture treatment.

In conclusion, WBV bouts with short rest intervals promoted cortical defect repair in OVX mice in terms of both bone volume and mineral density, which did not accompany further induction of angiogenesis but rather reduced large-sized vessels. Continuous WBV, despite having the same total number of vibratory cycles as WBV bouts with short rest intervals, failed to effectively promote defect repair to the same extent and was instead associated with an increase in large-sized angiogenic vessels. The enhanced outcomes of bone repair in WBV bouts with short rest intervals may be attributed to improved mechanosensitivity of osteogenic cells. Additionally, the differences in angiogenic vasculature between the two WBV treatments might potentially be associated with discrepancies in bone repair outcomes. Further studies are necessary to clarify the interaction between the effects of WBV on osteogenesis and angiogenesis in the context of bone repair. Notably, the capacity of bone marrow MSCs to differentiate towards osteogenic lineages and potentially toward endothelial lineages underscores their pivotal role in bone repair.[48,49] The prospective impacts of WBV on MSC behaviors, osteogenesis, angiogenesis, and their interconnections in osteoporosis introduce further complexity, warranting a comprehensive investigation.

ACKNOWLEDGMENTS

The synchrotron radiation experiments were performed at SPring-8 with the approval of the Japan Synchrotron Radiation Research Institute (JASRI) (proposal nos. 2017B1446, 2018B1107, 2019B1389, and 2021B1309). The authors would like to thank Drs. Kentaro Uesugi and Masato Hoshino (SPring-8/JASRI) for their valuable support and assistance throughout the synchrotron radiation experiments and Kelly Zammit, BVSc, from Edanz (https://jp.edanz.com/ac) for editing a draft of this manuscript. A part of this study was supported by a grant from the Suzuken Memorial Foundation (16-027).

Declaration of Interests

The authors declare that they have no conflicts of interest.

REFERENCES

1. Shiraki M, Kuroda T, Shiraki Y, et al. Effects of bone mineral density of the lumbar spine and prevalent vertebral fractures on the risk of immobility. Osteoporos Int. 2010;21:1545–1551.
2. Ström O, Borgström F, Kanis JA, et al. Osteoporosis: burden, health care provision and opportunities in the EU: a report prepared in collaboration with the International Osteoporosis Foundation (IOF) and the European Federation of Pharmaceutical Industry Associations (EFPIA). Arch Osteoporos. 2011;6:59–155.
3. Namkung-Matthai H, Appleyard R, Jansen J, et al. Osteoporosis influences the early period of fracture healing in a rat osteoporotic model. Bone. 2001;28:80–86.
4. Pang J, Ye M, Gu X, et al. Ovariectomy-induced osteopenia influences the middle and late periods of bone healing in a mouse femoral osteotomy model. Rejuvenation Res. 2015;18:356–365.
5. Cheung WH, Miclau T, Chow SK, et al. Fracture healing in osteoporotic bone. Injury. 2016;47(Suppl 2):S21–S26.
6. Johnell O, Kanis JA. An estimate of the worldwide prevalence and disability associated with osteoporotic fractures. Osteoporos Int. 2006;17:1726–1733.

7. Bliuc D, Nguyen ND, Milch VE, et al. Mortality risk associated with low-trauma osteoporotic fracture and subsequent fracture in men and women. JAMA. 2009;301:513–521.

8. Szczesny SE, Lee CS, Soslowsky LJ. Remodeling and repair of orthopedic tissue: role of mechanical loading and biologics. Am J Orthop. 2010;39:525–530.

9. Boerckel JD, Kolambkar YM, Stevens HY, et al. Effects of in vivo mechanical loading on large bone defect regeneration. J Orthop Res. 2012;30:1067–1075.

10. Barcik J, Ernst M, Buchholz T, et al. The absence of immediate stimulation delays bone healing. Bone. 2023:116834.

11. Gao H, Zhai M, Wang P, et al. Low-level mechanical vibration enhances osteoblastogenesis via a canonical Wnt signaling-associated mechanism. Mol Med Rep 2017;16:317–324.

12. Lu Y, Zhao Q, Liu Y, et al. Vibration loading promotes osteogenic differentiation of bone marrow-derived mesenchymal stem cells via p38 MAPK signaling pathway. J Biomech 2018;71:67–75.

13. Huang RP, Rubin CT, McLeod KJ. Changes in postural muscle dynamics as a function of age. J Gerontol A Biol Sci Med Sci. 1999;54:B352–B357.

14. Fritton SP, McLeod KJ, Rubin CT. Quantifying the strain history of bone: spatial uniformity and self-similarity of low-magnitude strains. J Biomech. 2000;33:317–325.

15. Wang J, Leung KS, Chow SK, Cheung WH. The effect of whole body vibration on fracture healing - a systematic review. Eur Cell Mater. 2017;34:108–127.

16. Wehrle E, Liedert A, Heilmann A, et al. The impact of low-magnitude high-frequency vibration on fracture healing is profoundly influenced by the oestrogen status in mice. Dis Model Mech. 2015;8:93–104.

17. Cheung WH, Sun MH, Zheng YP, et al. Stimulated angiogenesis for fracture healing augmented by low-magnitude, high-frequency vibration in a rat model-evaluation of pulsed-wave doppler, 3-D power Doppler ultrasonography and micro-CT microangiography. Ultrasound Med Biol. 2012;38:2120–2129.

18. Li W, Wang K, Liu Z, Ding W. HIF-1α change in serum and callus during fracture healing in ovariectomized mice. Int J Clin Exp Pathol. 2015;8:117–126.

19. Long F. Building strong bones: molecular regulation of the osteoblast lineage. Nat Rev Mol Cell Biol. 2011;13:27–38.

20. Maes C, Kobayashi T, Selig MK, et al. Osteoblast precursors, but not mature osteoblasts, move into developing and fractured bones along with invading blood vessels. Dev Cell.

2010;19:329–344.

21. Mundy GR, Chen D, Zhao M, et al. Growth regulatory factors and bone. Rev Endocr Metab Disord. 2001;2:105–115.

22. Marin-Cascales E, Alcaraz PE, Ramos-Campo DJ, et al. Whole-body vibration training and bone health in postmenopausal women: A systematic review and meta-analysis. Medicine (Baltimore). 2018;97:e11918.

23. Turner CH, Robling AG. Designing exercise regimens to increase bone strength. Exerc Sport Sci Rev. 2003;31:45–50.

24. Srinivasan S, Weimer DA, Agans SC, et al. Low-magnitude mechanical loading becomes osteogenic when rest is inserted between each load cycle. J Bone Miner Res. 2002;17:1613–1620.

25. Robling AG, Burr DB, Turner CH. Recovery periods restore mechanosensitivity to dynamically loaded bone. J Exp Biol. 2001;204:3389–3399.

26. LaMothe JM, Zernicke RF. Rest insertion combined with high-frequency loading enhances osteogenesis. J Appl Physiol. 2004;96:1788–1793.

27. Garman R, Gaudette G, Donahue LR, et al. Low-level accelerations applied in the absence of weight bearing can enhance trabecular bone formation. J Orthop Res.

2007;25:732–740.

28. Matsumoto T, Goto D. Effect of low-intensity whole-body vibration on bone defect repair and associated vascularization in mice. Med Biol Eng Comput. 2017;55:2257–2266.

29. Robling AG, Turner CH. Mechanotransduction in bone: genetic effects on mechanosensitivity in mice. Bone. 2002;31:562–569.

30. Matsumoto T, Itamochi S, Hashimoto Y. Effect of concurrent use of whole-body vibration and parathyroid hormone on bone structure and material properties of ovariectomized mice. Calcif Tissue Int. 2016;98:520–529.

31. Matsumoto T, Goto D, Sato S. Subtraction micro-computed tomography of angiogenesis and osteogenesis during bone repair using synchrotron radiation with a novel contrast agent. Lab Invest. 2013;93:1054–1063.

32. Doube M, Kłosowski MM, Arganda-Carreras I, et al. BoneJ: Free and extensible bone image analysis in ImageJ. Bone. 2010;47:1076–1079.

33. Shi HF, Cheung WH, Qin L, et al. Low-magnitude high-frequency vibration treatment augments fracture healing in ovariectomy-induced osteoporotic bone. Bone. 2010;46:1299–1305.

34. Matsumoto T, Sato D, Hashimoto Y. Individual and combined effects of noise-like whole-body vibration and parathyroid hormone treatment on bone defect repair in ovariectomized mice. Proc Inst Mech Eng H. 2016;230:30–38.

35. Uzer G, Pongkitwitoon S, Ete Chan M, Judex S. Vibration induced osteogenic commitment of mesenchymal stem cells is enhanced by cytoskeletal remodeling but not fluid shear. J Biomech. 2013;46:2296–2302.

36. Haffner-Luntzer M, Lackner I, Liedert A, et al. Effects of low-magnitude high-frequency vibration on osteoblasts are dependent on estrogen receptor α signaling and cytoskeletal remodeling. Biochem Biophys Res Commun. 2018;503:2678–2684.

37. Li H, Wu W, He X, et al. Applying vibration in early postmenopausal osteoporosis promotes osteogenic differentiation of bone marrow-derived mesenchymal stem cells and suppresses postmenopausal osteoporosis progression. Biosci Rep. 2019;39:BSR20191011.

38. Batra NN, Li YJ, Yellowley CE, et al. Effects of short-term recovery periods on fluid-induced signaling in osteoblastic cells. J Biomech. 2005;38:1909–1917.

39. Donahue SW, Donahue HJ, Jacobs CR. Osteoblastic cells have refractory periods for fluid-flow-induced intracellular calcium oscillations for short bouts of flow and display

multiple low-magnitude oscillations during long-term flow. J Biomech. 2003;36:35–43.

40. Huang C, Ness VP, Yang X, et al. Spatiotemporal analyses of osteogenesis and angiogenesis via intravital imaging in cranial bone defect repair. J Bone Miner Res. 2015;30:1217–1230.

41. Pries AR, Secomb TW. Making microvascular networks work: angiogenesis, remodeling, and pruning. Physiology (Bethesda). 2014;29:446–455.

42. Durand MJ, Ait-Aissa K, Gutterman DD. Regenerative Angiogenesis: Quality Over Quantity. Circ Res. 2017;120:1379–1380.

43. Chen Q, Wang Z, Yang C, et al. High resolution intravital photoacoustic microscopy reveals VEGF-induced bone regeneration in mouse tibia. Bone. 2023;167:116631.

44. Xie L, Jacobson JM, Choi ES, et al. Low-level mechanical vibrations can influence bone resorption and bone formation in the growing skeleton. Bone. 2006;39:1059–1066.

45. Rubinacci A, Marenzana M, Cavani F, et al. Ovariectomy sensitizes rat cortical bone to whole-body vibration. Calcif Tissue Int. 2008;82:316–326.

46. He YX, Zhang G, Pan XH, et al. Impaired bone healing pattern in mice with ovariectomy-induced osteoporosis: A drill-hole defect model. Bone. 2011;48:1388–1400.

47. Liu C, Cabahug-Zuckerman P, Stubbs C, et al. Mechanical loading promotes the

expansion of primitive osteoprogenitors and organizes matrix and vascular morphology in long bone defects. J Bone Miner Res. 2019;34:896–910.

48. Liu J, Liu C, Sun B, et al. Differentiation of rabbit bone mesenchymal stem cells into endothelial cells in vitro and promotion of defective bone regeneration in vivo. Cell Biochem Biophys. 2014;68:479–487.

49. Dan P, Velot É, Decot V, Menu P. The role of mechanical stimuli in the vascular differentiation of mesenchymal stem cells. J Cell Sci. 2015;128:2415–2422.

Table 1 Bone parameters

	day 7			day 14		
	sham	cWBV	rWBV	sham	cWBV	rWBV
B.Vf [%]	26.9 ± 4.7	23.0 ± 4.0	24.1 ± 7.6	44.0 ± 6.7	52.6 ± 7.3	59.6 ± 5.9**
B.Th [µm]	18.6 ± 1.9	18.2 ± 2.2	19.1 ± 4.3	43.0 ± 5.1	46.1 ± 4.7	47.7 ± 5.3
B.Sep [µm]	55.2 ± 14.6	54.8 ± 5.9	53.1 ± 4.5	90.7 ± 19.8	77.0 ± 17.4	62.2 ± 10.2**

B.Vf and B.Th differed between days 7 and 14 ($P < 0.01$) in every group.

B.Sep differed between days 7 and 14 in the sham ($P < 0.05$) and cWBV ($P < 0.01$) groups.

**$P < 0.01$ vs. the sham group on day 14.

cWBV, continuous whole-body vibration; rWBV, repeated bouts of whole-body vibration with short rest intervals; B.Vf, bone fraction volume; B.Th, bone thickness; B.Sep, bone spacing or thickness of the background.

Table 2 Blood vessel parameters

	day 7			day 14		
	sham	cWBV	rWBV	sham	cWBV	rWBV
V.Vf [%]	5.5 ± 1.9	5.7 ± 1.6	4.4 ± 1.7	4.0 ± 2.4	6.4 ± 3.3	2.8 ± 2.3
V.Th [µm]	26.6 ± 3.0	25.6 ± 3.3	23.4 ± 4.2	15.8 ± 3.1††	21.9 ± 6.3	12.4 ± 2.0$^{††, \#\#}$
V.N [/mm^3]	1679 ± 655	2256 ± 749	1859 ± 495	1163 ± 684	1366 ± 567†	758 ± 283††

$^{†}P < 0.05$, $^{††}P < 0.01$ vs. day 7.

$^{\#\#}P < 0.01$ vs. the cWBV group on day 14.

cWBV, continuous whole-body vibration; rWBV, repeated bouts of whole-body vibration with short rest intervals; V.Vf, vascular volume fraction; V.Th, vessel thickness; V.N, vessel number density.

Figure legends

Figure 1. Computed tomographic images of bone (gray) and blood vessels (red) in a cylindrical region (diameter, 495 μm; height, 110 μm) located in the tibial cortical bone defect on days 7 and 14. Bone regions are displayed as regions with mineral density > 0.5 g/cm^3. The lighter the gray, the higher the mineral density. On day 7, a woven-like bone structure was observed in every group. On day 14, bone regeneration advanced and blood vessels occupied a smaller space in the rWBV group than in the other two groups. In the cWBV group, thick blood vessels were observed at a relatively high frequency. The lengths of the orthogonal thick-line segments are all 100 μm. cWBV, continuous whole-body vibration; rWBV, repeated bouts of whole-body vibration with short rest intervals.

Figure 2. Percent distributions of bone volume versus bone mineral density in the cortical defect on days 7 and 14, where bone volume at each density value (bin width: 0.022 g/cm^3) is expressed as a percentage of the total volume with mineral density > 0.5 g/cm^3. On day 14, compared with the sham group, the rWBV group showed a low coefficient of variations and a trend toward low negative skewness, indicating advanced bone repair in terms of mineralization. cWBV, continuous

whole-body vibration; rWBV, repeated bouts of whole-body vibration with short rest intervals.

Figure 3. Vessel number density (V.N) in the cortical defect shown for the vessel thickness ranges of < 11.0 and > 11.0 µm on days 7 and 14. On day 7, V.N was higher or tended to be higher for > 11.0 µm thickness than < 11.0 µm thickness in every group. From days 7 to 14, V.N for > 11.0 µm thickness decreased and tended to decrease in the rWBV and cWBV groups, respectively, while V.N for < 11.0 µm thickness tended to decrease in the rWBV group. On day 14, V.N was higher for > 11.0 µm thickness than < 11.0 µm thickness in the sham and cWBV groups, but V.N was similar between the two thickness ranges in the rWBV group. cWBV, continuous whole-body vibration; rWBV, repeated bouts of whole-body vibration with short rest intervals.

Figure 4. Percent distributions of size-specific vessel number density (%V.N) in the cortical defect on days 7 and 14 are shown in boxplots. On day 14, the rWBV group had a dominant distribution of vessels with < 11.0-µm thickness, showing higher %V.N than the cWBV group and a trend toward higher %V.N than the sham group in the thickness of < 11.0 µm. Additionally, the cWBV group

showed a high heterogeneous distribution of vessel size, showing higher %V.N for relatively large-sized vessels compared with the other groups. cWBV, continuous whole-body vibration; rWBV, repeated bouts of whole-body vibration with short rest intervals.

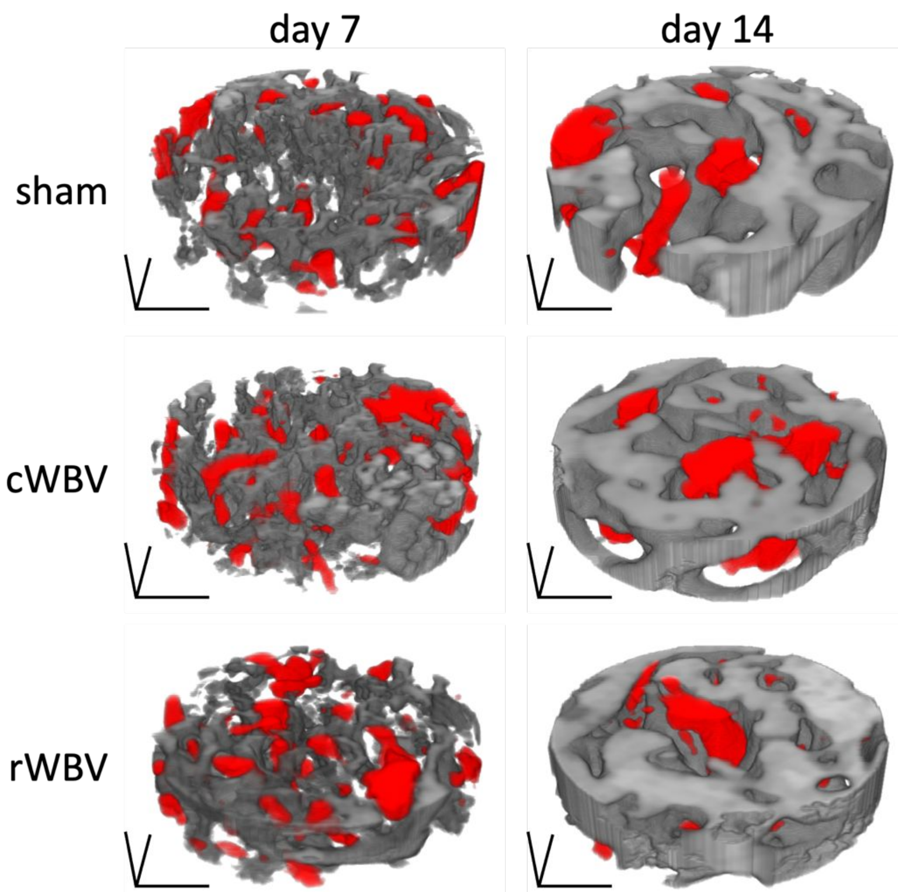

550

551 Figure 1

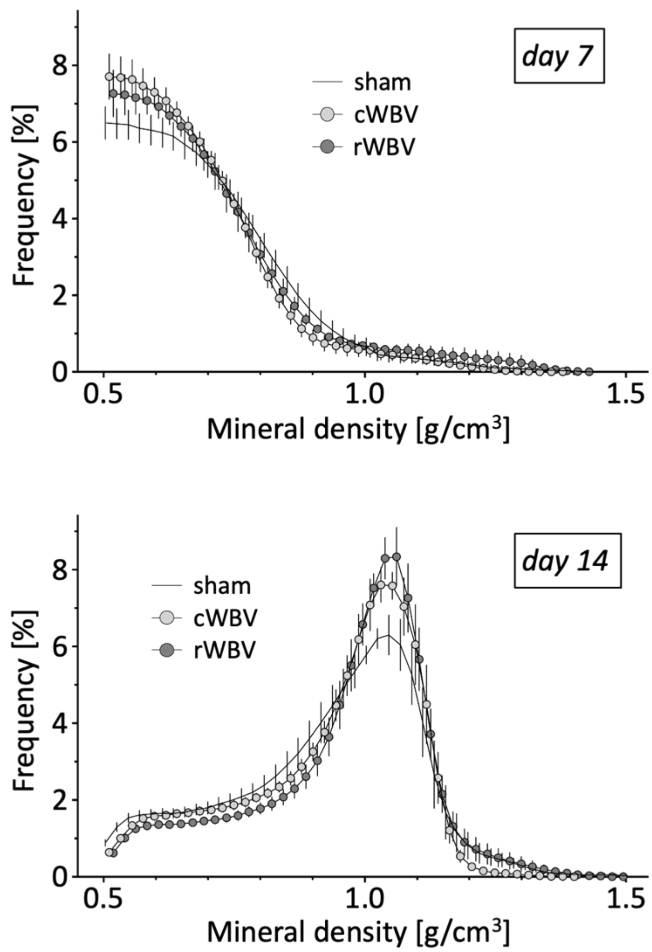

552

553 Figure 2

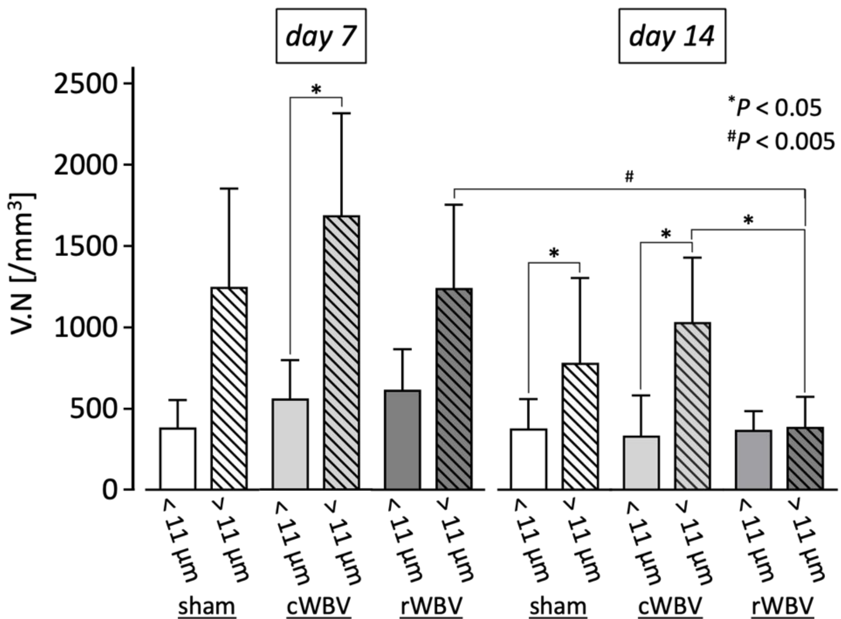

554

555 Figure 3

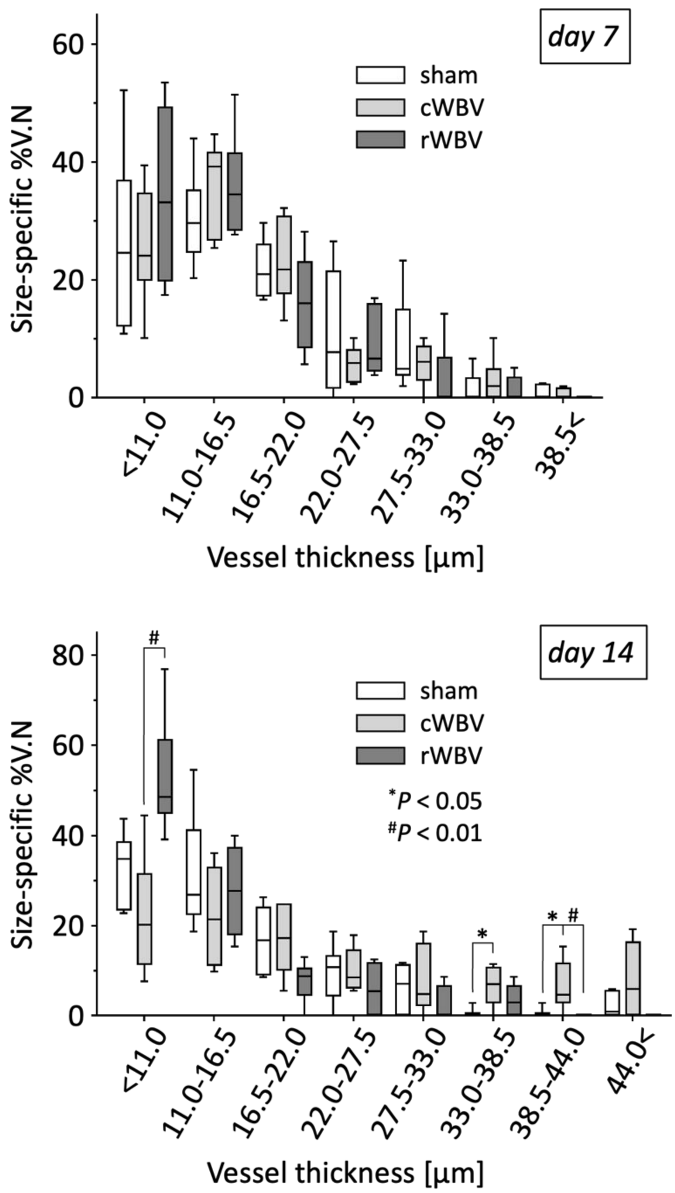

556

557 Figure 4

ARRIVE

The ARRIVE Guidelines Checklist

Animal Research: Reporting In Vivo Experiments

Carol Kilkenny[1], William J Browne[2], Innes C Cuthill[3], Michael Emerson[4] and Douglas G Altman[5]

[1]The National Centre for the Replacement, Refinement and Reduction of Animals in Research, London, UK, [2]School of Veterinary Science, University of Bristol, Bristol, UK, [3]School of Biological Sciences, University of Bristol, Bristol, UK, [4]National Heart and Lung Institute, Imperial College London, UK, [5]Centre for Statistics in Medicine, University of Oxford, Oxford, UK.

	ITEM	RECOMMENDATION	Section/ Paragraph
Title	1	Provide as accurate and concise a description of the content of the article as possible.	Title
Abstract	2	Provide an accurate summary of the background, research objectives, including details of the species or strain of animal used, key methods, principal findings and conclusions of the study.	Abstract
INTRODUCTION			
Background	3	a. Include sufficient scientific background (including relevant references to previous work) to understand the motivation and context for the study, and explain the experimental approach and rationale. b. Explain how and why the animal species and model being used can address the scientific objectives and, where appropriate, the study's relevance to human biology.	Introduction/P1-P4
Objectives	4	Clearly describe the primary and any secondary objectives of the study, or specific hypotheses being tested.	Introduction/P4
METHODS			
Ethical statement	5	Indicate the nature of the ethical review permissions, relevant licences (e.g. Animal [Scientific Procedures] Act 1986), and national or institutional guidelines for the care and use of animals, that cover the research.	Materials and methods/P1
Study design	6	For each experiment, give brief details of the study design including: a. The number of experimental and control groups. b. Any steps taken to minimise the effects of subjective bias when allocating animals to treatment (e.g. randomisation procedure) and when assessing results (e.g. if done, describe who was blinded and when). c. The experimental unit (e.g. a single animal, group or cage of animals). A time-line diagram or flow chart can be useful to illustrate how complex study designs were carried out.	Materials and methods/P3
Experimental procedures	7	For each experiment and each experimental group, including controls, provide precise details of all procedures carried out. For example: a. How (e.g. drug formulation and dose, site and route of administration, anaesthesia and analgesia used [including monitoring], surgical procedure, method of euthanasia). Provide details of any specialist equipment used, including supplier(s). b. When (e.g. time of day). c. Where (e.g. home cage, laboratory, water maze). d. Why (e.g. rationale for choice of specific anaesthetic, route of administration, drug dose used).	Materials and methods/P2-P5
Experimental animals	8	a. Provide details of the animals used, including species, strain, sex, developmental stage (e.g. mean or median age plus age range) and weight (e.g. mean or median weight plus weight range). b. Provide further relevant information such as the source of animals, international strain nomenclature, genetic modification status (e.g. knock-out or transgenic), genotype, health/immune status, drug or test naïve, previous procedures, etc.	Materials and methods/P2

Housing and husbandry	9	Provide details of: a. Housing (type of facility e.g. specific pathogen free [SPF]; type of cage or housing; bedding material; number of cage companions; tank shape and material etc. for fish). b. Husbandry conditions (e.g. breeding programme, light/dark cycle, temperature, quality of water etc for fish, type of food, access to food and water, environmental enrichment). c. Welfare-related assessments and interventions that were carried out prior to, during, or after the experiment.	Materials and methods/P 5
Sample size	10	a. Specify the total number of animals used in each experiment, and the number of animals in each experimental group. b. Explain how the number of animals was arrived at. Provide details of any sample size calculation used. c. Indicate the number of independent replications of each experiment, if relevant.	Materials and methods/P 2, P3
Allocating animals to experimental groups	11	a. Give full details of how animals were allocated to experimental groups, including randomisation or matching if done. b. Describe the order in which the animals in the different experimental groups were treated and assessed.	N/A
Experimental outcomes	12	Clearly define the primary and secondary experimental outcomes assessed (e.g. cell death, molecular markers, behavioural changes).	N/A
Statistical methods	13	a. Provide details of the statistical methods used for each analysis. b. Specify the unit of analysis for each dataset (e.g. single animal, group of animals, single neuron). c. Describe any methods used to assess whether the data met the assumptions of the statistical approach.	Materials and methods/P 11
RESULTS			
Baseline data	14	For each experimental group, report relevant characteristics and health status of animals (e.g. weight, microbiological status, and drug or test naïve) prior to treatment or testing. (This information can often be tabulated).	Results/P1
Numbers analysed	15	a. Report the number of animals in each group included in each analysis. Report absolute numbers (e.g. 10/20, not 50%[2]). b. If any animals or data were not included in the analysis, explain why.	Results/P1
Outcomes and estimation	16	Report the results for each analysis carried out, with a measure of precision (e.g. standard error or confidence interval).	Results/P2-P5
Adverse events	17	a. Give details of all important adverse events in each experimental group. b. Describe any modifications to the experimental protocols made to reduce adverse events.	N/A
DISCUSSION			
Interpretation/ scientific implications	18	a. Interpret the results, taking into account the study objectives and hypotheses, current theory and other relevant studies in the literature. b. Comment on the study limitations including any potential sources of bias, any limitations of the animal model, and the imprecision associated with the results[2]. c. Describe any implications of your experimental methods or findings for the replacement, refinement or reduction (the 3Rs) of the use of animals in research.	Discussion/ P3-P6
Generalisability/ translation	19	Comment on whether, and how, the findings of this study are likely to translate to other species or systems, including any relevance to human biology.	N/A
Funding	20	List all funding sources (including grant number) and the role of the funder(s) in the study.	Acknowledgments/P1

References:
1. Kilkenny C, Browne WJ, Cuthill IC, Emerson M, Altman DG (2010) Improving Bioscience Research Reporting: The ARRIVE Guidelines for Reporting Animal Research. *PLoS Biol* 8(6): e1000412. doi:10.1371/journal.pbio.1000412
2. Schulz KF, Altman DG, Moher D, the CONSORT Group (2010) CONSORT 2010 Statement: updated guidelines for reporting parallel group randomised trials. *BMJ* 340:c332.